Check for updates

19360592, ja, Downloaded from https://onlinelibrary.wiley.com/doi/10.1002/eco.2530 by Institut National De La Recherche, Wiley Online Library on [16/02/2023]. See the Terms and Conditions (https://onlinelibrary.wiley.com/terms-and-conditions) on Wiley Online Library for rules of use; OA articles are governed by the applicable Creative Commons License

Glowa Sarah E. (Orcid ID: 0000-0002-0711-6642)

Applying a 2D-Hydrodynamic Model to Estimate Fish Stranding Risk Downstream from a Hydropeaking Hydroelectric Station

Sarah E. Glowa[1,2], Andrea J. Kneale[1], Douglas A. Watkinson[1], Haitham K. Ghamry[1], Eva C. Enders[3] & Timothy D. Jardine[2]

[1]Fisheries and Oceans Canada, Freshwater Institute, Winnipeg, Manitoba, Canada
[2]University of Saskatchewan, Saskatoon, Saskatchewan, Canada
[3]Institut Nationale de la Recherche Scientifique, Eau Terre Environnement Research Centre, Québec, Québec, Canada

Correspondence: Sarah E. Glowa, Fisheries and Oceans Canada, Freshwater Institute, Winnipeg, Manitoba, Canada
Email: sarah.glowa@dfo-mpo.gc.ca

Keywords
Photogrammetry; River2D; wetted area; Saskatchewan River

Abstract

Fish stranding is of global concern with increasing hydropower operations using hydropeaking to respond to fluctuating energy demand. Determining the effects hydropeaking has on fish communities is challenging because fish stranding is dependent on riverscape features, such as topography, bathymetry, and substrate. By using a combination of physical habitat assessments, hydrodynamic modeling, and empirical data on fish stranding, we estimated the number of fish stranding over a five-month period for three model years in a large Prairie river. More specifically, we modelled how many fish potentially stranded during years 2019, 2020, and 2021 across a 16 km study reach downstream from E.B. Campbell Hydroelectric Station on the Saskatchewan River, Canada.

This article has been accepted for publication and undergone full peer review but has not been through the copyediting, typesetting, pagination and proofreading process which may lead to differences between this version and the Version of Record. Please cite this article as doi: 10.1002/eco.2530

This article is protected by copyright. All rights reserved.

Fish stranding densities calculated from data collected through remote photography and transect monitoring in 2021 were applied to the daily area subject to drying determined by the River2D hydrodynamic model. The cumulative area subject to change was 90.05 km^2, 53.02 km^2, and 80.74 km^2 for years 2019, 2020, and 2021, respectively, from June through to October. The highest number of stranded fish was estimated for year 2021, where estimates ranged from 89,800 to 1,638,000 individuals based on remote photography and transect monitoring fish stranding densities, respectively, 157 to 2,856 fish stranded per hectare. Our approach of estimating fish stranding on a large scale allows for a greater understanding of the impact hydropeaking has on fish communities and can be applied to other riverscapes threatened by hydropeaking.

1 | Introduction

The number of hydroelectric stations is increasing worldwide to meet the energy demands of a growing global population (Zarfl et al., 2015). Hydroelectric stations are part of renewable energy portfolios, but they subject river ecosystems to anthropogenic stressors such as flow regime alterations. Particularly, storage hydropeaking stations that use large reservoirs to hold water potential to convert to energy when needed (Vaca-Jiménez et al., 2020) can greatly alter a river's downstream flow regime. The daily hydropeaking cycle provides maximum power generation when power is required (e.g., during daytime hours) followed by minimal power generation when energy is not needed (e.g., at nighttime). Consequently, the wetted area of the downstream portion of the river may fluctuate substantially on a daily basis (Valentin et al., 1996), with hydropeaking impacts being seen at high intensities in the first few kilometers downstream from the hydroelectric station but the effects can be observed up to 40 km or further downstream (Hayes et al., 2022). One potential consequence of the daily, rapid change in wetted area is fish stranding (Larrieu et al., 2021).

Fish stranding occurs when the wetted area of the river declines in response to hydroelectric station down-ramping, causing fish to be beached or trapped from the main thalweg. Canada lacks regulations specific to hydropeaking operations but the Canadian *Fisheries Act* (Canadian Ministry of Justice, 2019) provides prohibitions against causing the death of fish, by means other than fishing (Section 34.4) and against causing the harmful alteration, disruption, or destruction of fish habitat (Section 35). Similarly, in the United States of America, there are no specific hydropeaking regulations but the *Clean Water Act* (Federal Water Pollution Control Act, 2002), the *Endangered Species Act* (ESA, 1973), and

This article is protected by copyright. All rights reserved.

19360592, ja, Downloaded from https://onlinelibrary.wiley.com/doi/10.1002/eco.2530 by Institut National De La Recherche, Wiley Online Library on [16/02/2023]. See the Terms and Conditions (https://onlinelibrary.wiley.com/terms-and-conditions) on Wiley Online Library for rules of use; OA articles are governed by the applicable Creative Commons License

the *Federal Power Act* (FPA, 1920) are applied to mitigate the effects of hydropeaking. While legislature in North America provides a basis to establish mitigation measures to prevent adverse environmental effects due to hydropeaking, a few European countries have legal regulations for hydropeaking flow limits (Moreira et al., 2019). Establishing mitigation measures for hydropeaking is challenging as there are no standardized methods for determining the extent of fish stranding across multiple kilometers of a riverscape, defined as all spatially and temporally heterogenous and/or homogenous areas connected by the river. Fish stranding assessments are typically conducted via observational surveys and/or microcosm and mesocosm experiments used to determine if fish stranding is a concern at a given river reach (Nagrodski et al., 2012; Auer et al., 2017; Führer et al., 2022). Identifying potential stranding locations is achievable through application of hydrodynamic modelling of the river reach. However, small scale fish stranding data can be challenging to upscale to the level of the riverscape. Some studies modelled the variation in wetted area and dewatering ramping rate to gauge fish stranding areas (Sauterleute et al., 2016; Juárez et al., 2019; Larrieu & Pasternack, 2021) and estimate risk of stranded fish with little or no fish stranding data collected from the specific study site (Tuhtan et al., 2012; Hauer et al., 2014; Casas-Mulet et al., 2016; Sauterleute et al., 2016; Burman et al., 2021).

The outputs of hydrodynamic models include the wetted area of a river at different discharges, which can subsequently be used to estimate stranding risk (Valentin et al. 1996) by identifying the dewatered areas with fish stranding potential (Tuhtan et al., 2012; Mandlburger et al., 2015; Vanzo et al., 2016; Juárez et al., 2019; Larrieu & Pasternack, 2021). By modeling the wetted area during the high and low discharge peak and over the course of the fish growing season, the change in wetted area available to fish during hydropeaking events can be calculated and matched to their life histories. For example, results from an earlier study showed higher stranding rates with increasing water temperatures (Glowa et al., 2022), suggesting a mid-summer peak in stranding potential that could coincide with highly variable discharges and the presence of young-of-the-year life stages. Combining this information with *in situ* fish stranding surveys, fish stranding can be quantified on a reach scale as well as upscaled to the riverscape.

Upscaling stranding estimates is challenging because the magnitude of fish stranding is dependent on geomorphological characteristics of the river, such as slope, channel shape, and substrate type (Glowa et al., 2022 ; Juárez et al., 2019). Consequently, fish stranding will vary within the riverscape (Young et al., 2011). Obtaining a detailed topographic map is necessary for accurate hydrodynamic modeling; however, surveying a river can be

This article is protected by copyright. All rights reserved.

19360592, ja, Downloaded from https://onlinelibrary.wiley.com/doi/10.1002/eco.2530 by Institut National De La Recherche, Wiley Online Library on [16/02/2023]. See the Terms and Conditions (https://onlinelibrary.wiley.com/terms-and-conditions) on Wiley Online Library for rules of use; OA articles are governed by the applicable Creative Commons License

challenging and expensive. One option is light detection and ranging (LiDAR) surveying, which generates an elevation model of both topography and bathymetry (Mandlburger et al., 2015) but this technique is costly (Aristizábal-Botero et al., 2021). Alternatively, photogrammetry from a remotely piloted aircraft system can be used to develop a cost-effective detailed digital elevation model (DEM), where photographs are connected using software that associates common distinguishable features in each respective photograph to develop a fluent picture of a study reach. Photogrammetry is capable of precision on a cm-scale (Colomina & Molina, 2014) allowing for a detailed map of a riverscape. Due to the water level changes associated with hydropeaking, a DEM developed at low water can capture elevations that will become inundated, representing the habitat available to fish communities when the water levels are higher. Considering the limited capabilities of photogrammetry in watered locations, additional surveying of the river bathymetry is needed. The combination of photogrammetry and bathymetry allows for topography under both high and low discharge conditions (Burman et al., 2021) resulting in a complete site elevation map. Additionally, a substrate map can be developed to further identify where fish stranding is more likely to occur. Our earlier work found that in the Saskatechwan River downstream of the E.B. Campbell hydroelectric station, a greater fish stranding potential occurred over finer substrates (Glowa et al., 2022), which is in contrast to other studies on smaller, alpine systems were fish were more likley strand in coarser substrate (Hauer et al., 2014).

By combining the information gained from physical habitat assessments, hydrodynamic modeling, and empirical data on fish stranding from time-lapse cameras and transect monitoring, we estimated the fish stranding potential across a 16 km reach downstream from E.B. Campbell Hydroelectric Station on the Saskatchewan River located in Saskatchewan, Canada. Specifically, our objectives were to (1) develop a two-dimensional hydrodynamic model based on a combination of photogrammetry and bathymetry survey data to estimate the changes in wetted area of the study reach, and (2) estimate overall fish stranding during a five-month period in three years (2019, 2020, and 2021, respectively) that represent average, low, and high discharge scenarios in the Saskatchewan River.

2 | Methods

2.1 | Study Site

The E.B. Campbell Hydroelectric Station has operated on a hydropeaking regime to offset daily peak energy demands since 1962 (Watkinson et al., 2020), subjecting the

This article is protected by copyright. All rights reserved.

19360592, ja, Downloaded from https://onlinelibrary.wiley.com/doi/10.1002/eco.2530 by Institut National De La Recherche, Wiley Online Library on [16/02/2023]. See the Terms and Conditions (https://onlinelibrary.wiley.com/terms-and-conditions) on Wiley Online Library for rules of use; OA articles are governed by the applicable Creative Commons License

downstream wetted habitat to unnatural changes in water level. The station is located in East-Central Saskatchewan on the Saskatchewan River. The Saskatchewan River has a mean annual regulated flow of ~420 $m^3 \cdot s^{-1}$ (ECCC 2022) and flows into the Saskatchewan River Delta, which spans an area of 10,000 km^2 and is the largest inland delta in North America (MacKinnon et al., 2015). The station has capacity to generate up to 1000 $m^3 \cdot s^{-1}$. Once 1000 $m^3 \cdot s^{-1}$ is exceeded hydropeaking is difficult or impossible for the operator to maintain and outflow matches incoming flow to the reservoir with additional flows bypassed through a spillway channel. The hydropeaking regime can result in daily discharge fluctuations from ~100 to 1,000 $m^3 \cdot s^{-1}$, resulting in daily water level changes ~1.5 m depending on proximity to station. Fisheries and Oceans Canada's Fish and Fish Habitat Protection Program enforced a minimum instantaneous discharge requirement of 75 $m^3 \cdot s^{-1}$ in 2004 (Enders et al., 2017) to reduce fish stranding, and the mean minimum daily discharge is 150 $m^3 \cdot s^{-1}$. The station is operated using a single peak discharge every 24 h, typically occurring from ~12:00 to 22:00, while minimum discharge occurs in the night from ~0:00 to 2:00.

The study site is located downstream of the E.B. Campbell Hydroelectric Station consisting of ~16 km of the river channel, with an average width of 480 m (Figure 1). Fish stranding was previously quantified at three study reaches (Glowa et al., 2022). Reach 1 is ~1 km long and located in the tail end of the spillway channel (N 53.69022 W 103.34913) that receives backwater from the main channel during high flows. Reach 2 is ~1 km long and located on the south shore and a mid-channel island ~9 km downstream of the hydroelectric station (N 53.71792 W 103.23237). Reach 3 is ~1.2 km long and located ~13 km downstream of the hydroelectric station (N 53.72514 W 103.17578). Additional fish stranding surveys were conducted at a local boat launch (N 53.692633 W 103.326204; Figure 1), ~1.3 km downstream of Reach 1.

2.2 | Photogrammetry

A remotely piloted aircraft system was deployed to assess the topography by means of photogrammetry to produce a DEM (Thi et al., 2020). Imagery was conducted using a DJI Phantom 4 RTK (real-time kinematic) remotely piloted aircraft system with a DJI-RTK 2 Mobile Station (Shenzhen, China). The remotely piloted aircraft system was programmed to fly predetermined flight plans that covered the ~16 km study site in three sections. Surveys were conducted by collecting multiple overlapping photographs with a 70% side and 80% frontal overlap (Javernick et al., 2014; Leon et al., 2015). Flights were conducted in

This article is protected by copyright. All rights reserved.

19360592, ja, Downloaded from https://onlinelibrary.wiley.com/doi/10.1002/eco.2530 by Institut National De La Recherche, Wiley Online Library on [16/02/2023]. See the Terms and Conditions (https://onlinelibrary.wiley.com/terms-and-conditions) on Wiley Online Library for rules of use; OA articles are governed by the applicable Creative Commons License

September 2020 when the discharges were <500 $m^3 \cdot s^{-1}$, averaging 375 $m^3 \cdot s^{-1}$. A total of 13 ground control points (GCP) were placed throughout the mapping reach and used as reference points to aid the RTK processing capabilities. All GCPs were surveyed with a Leica Viva Global Navigation Satellite System total station to determine a benchmark of location and elevation later referenced in the photogrammetry processing.

Aerial photography was processed using structure-from-motion (SfM) software (Agisoft Metashape Professional, St. Petersburg, Russia). Overlapping images of the site were used to develop a photogrammetry map; moreover, common points within images were defined to create a dense point cloud (Colomina & Molina, 2014). GCPs and the RTK locations of all photographs taken by the drone were applied to position the dense point cloud within a global coordinate system. A dense point cloud is all the common coordinates found within the overlapping images created by SfM software (Tinkham & Swayze, 2021). The dense point cloud was then used to create a detailed DEM (10.2 cm per pixel) and further processed to construct an orthomosaic image of the study reach.

2.3 | Hydroacoustic Surveys

Photogrammetry is limited in determining riverbed elevation below water; therefore, bathymetry surveys were required to obtain accurate water depth/bathymetry measurements to determine riverbed elevation for the wetted area. In August 2020, a MX Aquatic Habitat Echosounder (BioSonics, Seattle, WA, USA) was deployed to measure river water depth when discharges exceeded 600 $m^3 \cdot s^{-1}$, averaging 751 $m^3 \cdot s^{-1}$. The BioSonics MX Echosounder uses a single frequency (204.8 kHz, 8.4°) conical beam with a ping rate of five pings per second (pps), pulse length of 0.4 ms, and rising edge threshold of −30 dB to collect data on substrate and depth. Data was collected every ten pings (approximately every 7 m). The transducer was secured to a 5.5 m vessel at the midpoint via a solid cross beam base with an adjustable pole mount. The pole and transducer were lowered to 25–35 cm below the water surface and surveyed at 9–11 $km \cdot h^{-1}$. Hydroacoustic data was collected along contours parallel to the riverbanks. Distances between the tracks ranged from <10 m to >135 m apart (when islands are present). In total, ~200 km of track was surveyed.

Using BioSonics Visual Habitat software, the hydroacoustic data was standardized to account for the depth at which the echosounder's transducer was deployed. Substrate type was assigned based on hydroacoustic amplitude (dB) readings using a principal components

This article is protected by copyright. All rights reserved.

19360592, ja, Downloaded from https://onlinelibrary.wiley.com/doi/10.1002/eco.2530 by Institut National De La Recherche, Wiley Online Library on [16/02/2023]. See the Terms and Conditions (https://onlinelibrary.wiley.com/terms-and-conditions) on Wiley Online Library for rules of use; OA articles are governed by the applicable Creative Commons License

analysis in the BioSonics Visual Habitat software. The software defined four substrate types based on hardness. In total, 33,425 data points were exported.

To ground-truth the substrate types, physical surveys were conducted to associate the hydroacoustic amplitude to a substrate particle size using a modified Wentworth scale (Wentworth, 1922). The substrate data file was imported into ArcGIS Pro (Redlands, CA, USA) to define substrate locations. A total of ten coordinates were selected for each substrate type to be sampled on site. Coordinate locations were surveyed visually if riverbed was exposed or, if submerged, an Aqua-vu camera (Crosslake, MN, USA) was used. For consistency, a single observer categorized all substrate locations.

To measure water depth and velocity within a reach, a Teledyne RD Instruments (TRDI) RiverRay acoustic doppler current profiler (ADCP) (TRDI, Poway, CA, USA) was used in August 2020. The TRDI RiverRay is a 600 kHz ADCP with a phased array transducer, 30-degree beam angles, and an auto-adaptive configuration algorithm. A GPS sensor is embedded with 3 m horizontal and 5 m vertical accuracy. The TRDI RiverRay ADCP was deployed in a trimaran, tethered to the end of a pole projecting off the bow of a 6 m research vessel. This allowed the ADCP transducer to be positioned free and clear of the boat hull that can create velocity and water surface distortions, and to minimize rotation relative to the boat. Measurements were completed in accordance with the field and office procedures outlined in the Environment and Climate Change Canada *Measuring Discharge with Acoustic Doppler Current Profilers from a Moving Boat* (Environment Canada, 2013). Velocity measurements were conducted approximately 300–500 m apart. In total, 32 velocity measurements consisting of reciprocal transects with a total exposure time of 720 s or greater were recorded. Transects were collected using a uniform boat speed across the cross-section and consistent boat speeds among the transects. TRDI's real-time discharge data collection program WinRiver II software was used to operate the ADCP and check and verify commands. WinRiver II was also used to complete quality assurance and quality control steps and post-process discharge measurements according to WinRiver II Software User's Guide (Teledyne RD Instruments, 2016).

2.4 | River2D Model

River2D (www.river2d.ca) is a two-dimensional hydrodynamic and habitat model capable of estimating flows and fish habitat across a study reach (Ghanem, 1995). The model determines the physical habitat (depth and water velocity) throughout the site area at any given flow. The model uses the bed topography and roughness to simulate the water surface

This article is protected by copyright. All rights reserved.

19360592, ja, Downloaded from https://onlinelibrary.wiley.com/doi/10.1002/eco.2530 by Institut National De La Recherche, Wiley Online Library on [16/02/2023]. See the Terms and Conditions (https://onlinelibrary.wiley.com/terms-and-conditions) on Wiley Online Library for rules of use; OA articles are governed by the applicable Creative Commons License

elevation as flows change. Bathymetric data collected throughout the study area was completed without a reference to the water surface elevation (WSE) at the time of the survey. Therefore, while depth data was known, bed elevation and the WSE at the time of the survey were not. The riverbed topography was determined using hydroacoustic sampling data collected in 2020 via the MX Aquatic Habitat Echosounder and TRDI RiverRay ADCP, WSE data from Water Survey of Canada (WSC) hydrometric station (05KD003) located 3.75 km downstream the hydroelectric station, and additional data from hydroacoustic sampling completed in 2006 (Watkinson et al., 2020). Calculations used to define the riverbed elevation are provided in the supplementary material.

To determine the wetted area and its daily change associated with a single daily hydropeak for the study site, the model was run at various discharges to cover all potential hydroelectric station outputs. A steady-state solution was sought for each discharge, the simulation iterations were still moderated by time increments and a final time was used to end the simulation and reach the steady-state solution. The objective was to reach the steady-state solution with as few calculations as possible while remaining stable under any discharge circumstances. Discharge was incremented for best representation of all possible flows. Discharges ranging from 70–260 $m^3 \cdot s^{-1}$ were modelled in 5 $m^3 \cdot s^{-1}$ increments, those from 270–1,100 $m^3 \cdot s^{-1}$ were modelled in 10 $m^3 \cdot s^{-1}$ increments, and those from 1150–2,200 $m^3 \cdot s^{-1}$ were modeled in 50 $m^3 \cdot s^{-1}$ increments. We did not calculate wetted area above 2,200 $m^3 \cdot s^{-1}$ because daily discharges above this value represent full inundation of the study reach (MacKinnon et al. 2016) and this value was exceeded in only 68 of the 20,947 daily observations in the gauge record (05KD003 Saskatchewan River below Tobin Lake (Environment Canada, 2015). The obtained wetted area for each discharge was used in a matrix of daily changes in wetted area, calculated from the maximum wetted area minus the minimum wetted area for all discharge scenarios. Matrix values represent the change in wetted area, which is the area prone to fish stranding. These areas of fish stranding potential are characterised by the drying of available habitat due to hydropeaking events, when the maximum discharge receded to the minimum discharge and fish were subjected to stranding on shores or in isolated pools that became disconnected from the main thalweg.

The River2D model interpreted the roughness height of the riverscape, developing a roughness map of the ~16 km study reach (Figure 2). Roughness height was defined using the bathymetry ground-truthing hydroacoustic amplitude and the orthomosaic image, visually defining substrate types where hydroacoustic amplitude was not defined. Substrate particle size was assessed using a modified Wentworth scale; sand 0.06–2 mm, pebble 2–64 mm,

This article is protected by copyright. All rights reserved.

19360592, ja, Downloaded from https://onlinelibrary.wiley.com/doi/10.1002/eco.2530 by Institut National De La Recherche, Wiley Online Library on [16/02/2023]. See the Terms and Conditions (https://onlinelibrary.wiley.com/terms-and-conditions) on Wiley Online Library for rules of use; OA articles are governed by the applicable Creative Commons License

cobble 64–256 mm and boulder 256–1000mm (Wentworth 1922). The substrate types were then given a roughness value determined as the average particle size (hard packed substrate was based on the lower value of the cobble scale; this is due to the bathymetry substrate typing not always clearly defining substrate as cobble but a mixture of substrates of lesser particle size); fine sand 0.0013 m, pebble 0.033 m, hard packed substrate 0.064 m, boulder 0.628 m, vegetation 0.628 m and forested area 0.9 m (Chow, 1959).

For the hydrodynamic simulations using the River2D model, the finite element grid intensities were designed primarily to meet the requirements for reasonable accuracy and execution time. We applied 5, 15 and 25 meter grids. The computationally generated meshes were created in an unstructured fashion and the primary criterion for refinement was topographic matching. Typically, the river reach was first defined by overlaying the entire surveyed area with a uniform spacing of nodes. Additional nodes were later placed around specific channel features or locations within the modelled area considered important to the hydraulics and habitat of the reach(es) of the study. Care was taken to avoid dramatic changes in discretization while changing from one density to another.

2.5 | Yearly Fish Stranding Model

Fish stranding was modeled for three years representing an average, low, and high flow year. 2019 represented an average flow year (median discharge = 471 $m^3 \cdot s^{-1}$; Figure 3), with two seasonal peaks resulting from snow/ice melt in the local Prairie region in May followed by snow/ice melt from the Rocky Mountains, Alberta reaching the station in July (Enders et al., 2017), and discharge exceeded 1,000 $m^3 \cdot s^{-1}$ 47 times (Table 1). 2021 exemplified a low flow year (median discharge 309 $m^3 \cdot s^{-1}$; Figure 3), only reaching 1,000 $m^3 \cdot s^{-1}$ for approximately four days in the summer and the spillway was not operated, while on multiple occasions discharge dropped <100 $m^3 \cdot s^{-1}$ (15 times, Table 1). 2020 was characterized as a high flow year (median discharge 560 $m^3 \cdot s^{-1}$; Figure 2), where the spillway outlet was opened in response to high discharges exceeding 1,000 $m^3 \cdot s^{-1}$ for approximately three months (75 times, Table 1). During spillway operation, hydropeaking is greatly reduced (Table 1, Figure 3).

The daily maximum and minimum discharges were determined for the study period (June 1 – October 31) of the three example years. Subsequently, the change in wetted area was identified by applying the change in wetted area matrix created using the River2D model. All daily maximum and minimum discharges were rounded to the nearest 5 $m^3 \cdot s^{-1}$ for

This article is protected by copyright. All rights reserved.

19360592, ja, Downloaded from https://onlinelibrary.wiley.com/doi/10.1002/eco.2530 by Institut National De La Recherche, Wiley Online Library on [16/02/2023]. See the Terms and Conditions (https://onlinelibrary.wiley.com/terms-and-conditions) on Wiley Online Library for rules of use; OA articles are governed by the applicable Creative Commons License

discharges <260 $m^3 \cdot s^{-1}$ and 10 $m^3 \cdot s^{-1}$ for discharges >260 $m^3 \cdot s^{-1}$. The resulting change in wetted area represented the total area of fish stranding potential during the open water season.

2.6 | Fish Stranding

Two methodologies were performed during 2021 to quantify fish stranding occurring at E.B. Campbell hydroelectric station. The data collected was applied to the total area of fish stranding potential to estimate the number of stranded fish during the open water season. Fish stranding was monitored using remote photography conducted in 2021 from June to October (Glowa et al., 2022). A total of 45 downward facing cameras were placed randomly throughout three reaches, 15 cameras per reach. These time lapse trail cameras (Boly trail camera, model 2G2060-D, Victoriaville, QC, Canada) were set to take images on a 30-minute interval continuously for the study period, to capture fish stranding associated with the hydropeaking regime. All images were inspected for stranded fish. The cameras captured an area ranging from 6.50–7.26 m^2 of the riverbed in each image, average area of 6.91 m^2. A total of 3212 inundation and drying events were captured by the cameras, collectively surveying 23,800 m^2, and observed a total of 59 fish. In addition, transect monitoring was conducted once a month from June to October 2021 (Glowa et al., 2022). A total of 299 transects were walked over the five months, ranging in length from 44–420 m. Transects walks were conducted in the early morning when water levels were lowest to observe fish stranding ~1.5 m on either side of the surveying line. The transect survey area was calculated by multiplying the total length of a given transect by 3 m (i.e., 1.5 m either side of the transect). A total of 8198.5 m of transect walks were completed, covering a complete survey area of 116,989 m^2 a total of 2,325 small-bodied fish were found (Table 2).

Daily fish stranding densities (fish$\cdot m^{-2}$) were calculated from remote photography and transect monitoring observations. Transect monitoring observations were specific to the day the survey was conducted. Daily fish stranding density was calculated by dividing the daily number of stranded fish by the area surveyed for each survey method.

Fish stranding densities obtained from remote photography and transect monitoring were multiplied by the fish stranding area determined by River2D to estimate the number of stranded fish for each of the three flow years. A generalized linear model (GLM), fit with the glm function in R version 2.10.0 (R Development Core Team, 2010), was used to determine whether this estimate could be done for the entire study area or whether it needed to be adjusted by time of year or reach. The GLM used the calculated fish stranding densities as the

This article is protected by copyright. All rights reserved.

19360592, ja, Downloaded from https://onlinelibrary.wiley.com/doi/10.1002/eco.2530 by Institut National De La Recherche, Wiley Online Library on [16/02/2023]. See the Terms and Conditions (https://onlinelibrary.wiley.com/terms-and-conditions) on Wiley Online Library for rules of use; OA articles are governed by the applicable Creative Commons License

response variable and predictor variables were surveying month and the reach the stranded fish was observed. Due to a high volume of zero values and to reduce heteroscedasticity in the model, a value of one was added to all datapoints before log transformation of fish stranding densities. Based on the outcome of this analysis (see Results), a monthly estimate was made based on monthly fish stranding densities (remote photography: 0.0002, 0.0056, 0.0014, 0.0025, 0.0007 fish·m^{-2} and transect monitoring: 0.00004, 0.0919, 0.0004, 0.0005, 0.0002 fish·m^{-2} for June, July, August, September, and October respectively).

3 | Results

3.1 | Changes in Wetted Area

The highest discharge modelled of 2,200 $m^3 \cdot s^{-1}$ resulted in 5.7 km^2 wetted area over the 16 km long river reach in the Saskatchewan River downstream of the E.B. Campbell Hydroelectric Station (Figure 4a), whereas the lowest modelled discharge of 70 $m^3 \cdot s^{-1}$ resulted in 4.2 km^2 wetted area (Figure 4b). This corresponded to a maximum depth change of 3.9 m, resulting from a maximum depth of 8.93 m during a discharge of 2,200 $m^3 \cdot s^{-1}$ and a maximum depth of 5.03 m at 70 $m^3 \cdot s^{-1}$ (Figure 4).

The highest mean daily change in wetted area of 0.6 km^2 was observed in 2019 (Table 3, Figure 5). In comparison, the lowest mean daily change in wetted area of 0.3 km^2 was observed in 2020 (Table 3, Figure 5).

Based on calculations performed in River2D, fine sand covered 0.11 km^2, pebble covered 0.86 km^2, hardpacked sediment covered 2.42 km^2, boulder covered 2.62 km^2, vegetation covered 2.57 km^2, and forest covered 0.13 km^2 of the study reach (Figure 6). 40% of the study reach was covered by small particle substrate (fine sand, pebble, and hard packed sediment) and 30% was composed of large particle sized substrate (boulder). The remaining area was defined as either vegetation or forested area (30%). Smaller particle sizes were generally in greater proportions further downstream from the station, while large particle sizes were more greatly congregated by the hydroelectric station (Figure 6). Fish stranding occurred in greater numbers further downstream from the station, for example, 279, 322, and 1,767 stranded fish were observed in remote photography and transect monitoring combined at Reach 1, Reach 2, and Reach 3, respectively.

This article is protected by copyright. All rights reserved.

19360592, ja, Downloaded from https://onlinelibrary.wiley.com/doi/10.1002/eco.2530 by Institut National De La Recherche, Wiley Online Library on [16/02/2023]. See the Terms and Conditions (https://onlinelibrary.wiley.com/terms-and-conditions) on Wiley Online Library for rules of use; OA articles are governed by the applicable Creative Commons License

3.2 | Fish Stranding Estimates

There were significant effects of month and reach on fish stranding density, with the month of July different from all other months and reaches 2 and 3 different from reach 1 (Figure 7; Table 4). The R^2 value of the model was 0.05, suggesting that month and reach only explained 5% of the variability of the data. However, since the July mean was far larger than the other months (more than double in remote photography, more than two orders of magnitude in transects), the number of stranded fish for each flow year was estimated monthly. Remote photography fish stranding estimates resulted in 158,200, 89,800, and 170,700 stranded fish for 2019, 2020, and 2021, respectively (Table 5). Transect monitoring fish stranding densities resulted in higher fish stranding numbers with 1,082,500, 194,800, and 1,638,000 stranded fish for 2019, 2020, and 2021, respectively (Table 5).

4 | Discussion

4.1 | Estimating Fish Stranding

This study used a combination of hydrodynamic modelling and fish stranding observations to estimate the number of fish stranded over five months in a large river that is subject to hydropeaking. The available wetted area downstream of the hydroelectric station is dependent on the daily hydropeaking regime, which is driven by energy demand (Valentin et al., 1996; Almeida et al., 2020), as well as the seasonal hydrograph. By analysing the daily hydropeaking regime, we determined the associated changes in wetted area allowing for a better understanding of fish stranding potential (Larrieu et al., 2021). Applying site-specific fish stranding densities obtained from two different survey techniques (i.e., remote photography and transect monitoring), 89,800 to 1,638,000 fish were estimated to have stranded from June 1st to October 31st for the example flow years; suggesting 157 to 2,856 fish stranded per hectare.

Fish stranding estimates for both sampling methods, remote photography and transect monitoring, were highest for the low flow year, followed by average and high flow years. The low flow year resulted in less water being available for storage in the upstream reservoir, preventing the operator from maximizing the high daily discharges during hydropeaking (Hayes et al., 2019). River channel morphology influences change in wetted area with increasing discharges. The largest wetted area changes occur across the range of lower flows as typically the bank becomes stepper near bank full and wetted area changes are less pronounced with increases in discharge (Figure 4). More stranding is expected in years when

This article is protected by copyright. All rights reserved.

19360592, ja, Downloaded from https://onlinelibrary.wiley.com/doi/10.1002/eco.2530 by Institut National De La Recherche, Wiley Online Library on [16/02/2023]. See the Terms and Conditions (https://onlinelibrary.wiley.com/terms-and-conditions) on Wiley Online Library for rules of use; OA articles are governed by the applicable Creative Commons License

the difference between high and low discharges in a given day results in the most change in wetted area. During an average flow year, the hydropeaking regime follows the energy demands as a result of optimal water storage. Consequently, the average daily change in discharge for an average flow year (2019) is greater than 2020 and 2021 (Figure 5). During a high flow year, the operator is limited by the capacity to store water (Almeida et al., 2020) and the difference between daily high and low discharges are decreased for much of the season as excess water is released through the spillway (Moreira et al., 2019) (Figure 5). As a result, there is less change in wetted area and thus, less stranding potential. It is important to note that the River2D model used in this study did not incorporate the complete spillway channel, which is composed of a series of disconnected pools that can lead to fish stranding; therefore, the wetted area may be underestimated when flows exceed 1,000 $m^3 \cdot s^{-1}$. These disconnected pools may minimize stranding by providing refuges to fish until the next flow peak; however, the water level of these pools fluctuates with the hydropeaking of the station and additional stranding may occur in the area subject to drying around the pools. This, combined with an additional ~40 km downstream of the study reach where water levels fluctuate daily and strandings may occur (Smith et al., 2016), means that our estimate of overall stranding is likely an underestimate of the fish stranding that occurs.

Monthly fish stranding can be influenced by variation in temperature leading to increased stranding in warmer months (Glowa et al., 2022). Temperature is known to affect fish behaviour, leading to fish occupying warmer nearshore environments and can result in fish being more susceptible to stranding (Korman & Campana, 2009). Stranding is likely greatest at times when warmest temperatures coincide with periods of maximum daily water level change due to hydropeaking, such as occurred in July 2021. Furthermore, the timing of increased stranding can be associated with fish life history for the life-stage and species (Nagrodski et al., 2012), resulting in a greater potential for stranded fish during certain months. Within our study, we observed a large number of White Sucker (*Catostomus commersonii*) stranded during July (n = 1,627, Table 2), resulting in an increased fish stranding density estimate in this month. White Sucker spawn in spring (April to early May), in small gravel and flowing water (Begley et al., 2018) making the Saskatchewan River an ideal spawning location. There is an increase of White Sucker numbers in July as the young-of-year emerge and occupy the river, subjecting them to potential stranding (Begley, et al. 2018). The majority of White Sucker we found stranded were young-of-the-year suggesting that in July the White Sucker is likely abundant in this month and the young-of-the-year the

This article is protected by copyright. All rights reserved.

19360592, ja, Downloaded from https://onlinelibrary.wiley.com/doi/10.1002/eco.2530 by Institut National De La Recherche, Wiley Online Library on [16/02/2023]. See the Terms and Conditions (https://onlinelibrary.wiley.com/terms-and-conditions) on Wiley Online Library for rules of use; OA articles are governed by the applicable Creative Commons License

most vulnerable to fish stranding. As White Sucker grow throughout the ice-free season, they become less susceptible to fish stranding (Moreira et al., 2020).

4.2 | Limitations

The River2D model was limited at Reach 1 due to the challenging terrain. Reach 1 was inaccessible by boat and therefore bathymetry surveys could not be conducted in this area. Since the only riverbed elevation data available for Reach 1 was collected via photogrammetry, the riverbed elevation used in the model for areas covered by water was the water surface elevation at the time of mapping. Therefore, the model is missing a portion of the change in wetted area at Reach 1. This could result in an underestimation of wetted area for this reach as pools in the spillway do not always drain dry.

It is important to note that the fish stranding densities were calculated based on fish stranding data recorded during 2021, which was a low flow year. Fish stranding densities were assumed to be the same during average and high flow years. The remote cameras were placed at elevations between 271–284 m that captured drying and wetting of habitat for the peak discharges between 245–1,088 $m^3 \cdot s^{-1}$ witnessed in 2021 (Figure 4). Since discharges in this reach can range up to >2,200 $m^3 \cdot s^{-1}$ in years with higher water levels, such as 2020, more information is needed about stranding potential on the river margins that are wetted at these high flows. During these high flows hydropeaking is minimal, and the risk of fish stranding reduced, but when discharge decreases stranding may occur with hydropeaking resuming when discharge is closer to 1,000 $m^3 \cdot s^{-1}$ in our study reach.

Yearly recruitment may vary between years due to difference in discharge and water level, suggesting that the number of stranded fish observed during our low water levels may be less than what would potentially be seen in high water level years (Sammons & Bettoli, 2011). Subsequently, additional research is needed during average and high flow years to better understand fish stranding during these conditions.

Currently, the model considers all locations subject to drying as equal area for fish stranding potential. Future modelling could aim to weigh the risk of fish stranding based on topographic features, such as substrate type and habitat suitability indices.

4.3 | Substrate

Substrates with finer particle sizes were associated with an increased risk of fish stranding (Figure 6, Glowa et al., 2022). Substrates of fine particles are subject to continuous distribution changes as hydropeaking waters rise and fall, creating pools and potholes where fish tend to get trapped and strand (Irvine et al., 2009; Tuhtan et al., 2012; Puffer et al., 2017; Moreira et al., 2020; Glowa et al., 2022). The occurrence of pools and potholes was more

This article is protected by copyright. All rights reserved.

19360592, ja, Downloaded from https://onlinelibrary.wiley.com/doi/10.1002/eco.2530 by Institut National De La Recherche, Wiley Online Library on [16/02/2023]. See the Terms and Conditions (https://onlinelibrary.wiley.com/terms-and-conditions) on Wiley Online Library for rules of use; OA articles are governed by the applicable Creative Commons License

common on finer substrates (Glowa et al., 2022). Here, we estimated that finer substrates composed 40% of the study reach, suggesting a greater risk of stranding on these areas. There is a greater proportion of smaller particle substrates further downstream (Figure 6), likely a result of the deposition of fine substrates in the lower slope Reach 2 and 3 (Batalla et al., 2021), and minimal sand and clay replenishment from the reservoir trapping these finer particles from upstream (Bruno et al., 2009; Smith et al., 2016; Enders et al., 2017). Consequently, we observed a greater number of fish being stranded further away from the station on areas with finer substrate.

4.4 | Significance

Fish stranding due to the hydropeaking of E.B. Campbell Hydroelectric Station has been identified as a significant issue by the community of Cumberland House on the Saskatchewan River (Abu et al., 2020; Green et al., 2020; Mihalicz et al., 2019). A previous study estimating the number of stranded fish at E.B. Campbell Hydroelectric Station within the lower portion of the spillway channel (comparable to our study Reach 1) found up to 9,122 fish were stranded within ~56,862 m^2 from May 2009 through October 2009 (Nelson et al., 2009). An additional study conducted in four days in November 2010 predicted up to 1,162 fish were stranded daily in ~56,862 m^2 downstream from the station and the most abundant species discovered was Cisco (*Coregonus artedi*) with 49 identified out of 120 stranded fish (Nelson, 2010), while during our sampling we identified 16 Cisco out of 2,343 stranded fish. This suggests that the spawning season might influence the risk of stranding since Cisco are fall spawners (Stewart & Watkinson, 2004). The Saskatchewan River is home to a diverse fish community and is important for subsistence and recreational fisheries (Green et al., 2016). These fisheries have been threatened with a noticeable decrease in overall fish abundance (Abu et al., 2020). While nearly all the stranded population in our study consisted of juveniles and small-bodied species, explaining lower abundances downstream from the dam (Enders et al. 2017), some of the stranded population consisted of juveniles of highly valued species (Glowa et al., 2022). For example, 1.85% of stranded fish recorded during transect monitoring were Walleye (*Sander vitreus*) (Table 2). Using the 2021 transect monitoring reach specific estimate (1,638,000, Table 5), an estimated 27,400 Walleye were stranded between June and October 2021.

4.5 | Management

Th approach of modelling fish stranding downstream from a large hydropeaking hydroelectric station allowed for a better understanding of the extent of fish stranding occurring in the study reach, which has important management implications. We observed

This article is protected by copyright. All rights reserved.

19360592, ja, Downloaded from https://onlinelibrary.wiley.com/doi/10.1002/eco.2530 by Institut National De La Recherche, Wiley Online Library on [16/02/2023]. See the Terms and Conditions (https://onlinelibrary.wiley.com/terms-and-conditions) on Wiley Online Library for rules of use; OA articles are governed by the applicable Creative Commons License

greater stranding in the month of July, which is likely correlated to the occurrence of large numbers of young-of-the-year fish that have a higher stranding potential due to their abundance and habitat selection. Reducing or eliminating stranding during periods of time predicted to have higher stranding could mitigate stranding risk (e.g. July). Subsequently, operational approaches could be developed to limit hydropeaking during this period. If minimum flows are not lower than the natural 95% exceedance flows pre-dam construction the hydropeaking would be reduced and would limit stranding risks (Watkinson et al., 2020). Limiting the amplitude of the hydrograph (Batalla et al., 2021) could allow for power generation, but reduce the cumulative change in wetted area and reduce stranding (Watkinson et al., 2020). Additionally, an approach such as 'hydropeak free-weekends' can reduce the area for stranding greatly over the course of a month but can limit the generating stations electrical generation, which in return affects revenue (Batalla et al., 2021). We found presence of young-of-the-year fish greatly influenced the stranding rate, and if mitigation is applied to months with higher numbers of young-of-the-year fish, the risk of stranding can be reduced by implementing a minimum flow and reducing ramping rates (Hayes et al., 2019). Additionally, reducing the up- and down-ramping of the station may result in increased time for fish to seek new stable habitat reducing the number of fish stranding (Antonetti et al., 2022); however, Glowa et al. (2022) found that the ramping rate did not affect fish stranding potential.

5 | Conclusions

Hydrodynamic modelling combined with fish stranding densities, obtained from remote photography and transect monitoring, is a valuable concept to assess fish stranding potential and estimate the number of stranded fish at a riverscape scale. This working concept was successful in determining what months and years that fish are most at risk for stranding based on daily variations in discharge from hydropeaking. We estimated higher numbers of stranded fish in a low flow year when hydropeaking was limited overall but high in July, a month of increased stranding density. We observed great variability in estimating the number of fish stranding caused by hydropeaking operations across the studied flow years, due to the irregularity in fish stranding densities and changes in wetted area. Understanding when the potential for fish stranding is high allows hydropeaking operators to potentially alter their water release schedules to reduce fish stranding.

This article is protected by copyright. All rights reserved.

19360592, ja, Downloaded from https://onlinelibrary.wiley.com/doi/10.1002/eco.2530 by Institut National De La Recherche, Wiley Online Library on [16/02/2023]. See the Terms and Conditions (https://onlinelibrary.wiley.com/terms-and-conditions) on Wiley Online Library for rules of use; OA articles are governed by the applicable Creative Commons License

Acknowledgements

This study was financially supported by Fisheries and Oceans Canada's Freshwater Habitat Science Initiative (FHIN). We would like to thank Colin Kovachik, Doug Leroux, and Peter Johnson for help with field data collection.

Data Availability Statement

The data that support the findings of this study are available from the corresponding author, Sarah E. Glowa, upon reasonable request.

References

Abu, R., Reed, M. G., & Jardine, T. D. (2020). Using two-eyed seeing to bridge Western science and Indigenous knowledge systems and understand long-term change in the Saskatchewan River Delta, Canada. *International Journal of Water Resources Development*, *36*(5), 757–776. https://doi.org/10.1080/07900627.2018.1558050

Almeida, R. M., Hamilton, S. K., Rosi, E. J., Barros, N., Doria, C. R. C., Flecker, A. S., Fleischmann, A. S., Reisinger, A. J., & Roland, F. (2020). Hydropeaking Operations of Two Run-of-River Mega-Dams Alter Downstream Hydrology of the Largest Amazon Tributary. *Frontiers in Environmental Science*, *8*. https://doi.org/10.3389/FENVS.2020.00120/FULL

Antonetti, M., Hoppler, L., Tonolla, D., Vanzo, D., Schmid, M., & Doering, M. (2022). Integrating two-dimensional water temperature simulations into a fish habitat model to improve hydro- and thermopeaking impact assessment. *River Research and Applications*. https://doi.org/10.1002/RRA.4043

Aristizábal-Botero, Á., Páez-Pérez, D., Realpe, E., & Vanschoenwinkel, B. (2021). Mapping microhabitat structure and connectivity on a tropical inselberg using UAV remote sensing. *Progress in Physical Geography*, *45*(3), 427–445. https://doi.org/10.1177/0309133320964327

Auer, S., Zeiringer, B., Führer, S., Tonolla, D., & Schmutz, S. (2017). Effects of river bank heterogeneity and time of day on drift and stranding of juvenile European grayling (Thymallus thymallus L.) caused by hydropeaking. *Science of the Total Environment*, *575*, 1515–1521. https://doi.org/10.1016/j.scitotenv.2016.10.029

Batalla, R. J., Gibbins, C. N., Alcázar, A., Brasington, J., Buendia, C., Garcia, C., Llena, M., López, R., Palau, A., Rennie, C., Wheaton, J. M., & Vericat, D. (2021). Hydropeaked rivers need attention. *Environmental Research Letters*, *16*(2), 021001. https://doi.org/10.1088/1748-9326/ABCE26

Begley, M., Coghlan, S. M., & Zydlewski, J. (2018). Modeling White Sucker (Catostomus commersonii) populations to assess commercial harvest influence on age structure. *Https://Doi.Org/10.1080/02705060.2018.1496951*, *33*(1), 413–428. https://doi.org/10.1080/02705060.2018.1496951

Bruno, M. C., Maiolini, B., Carolli, M., & Silveri, L. (2009). Impact of hydropeaking on hyporheic invertebrates in an Alpine stream (Trentino, Italy). *International Journal of Limnology*, *45*(3), 157–170. https://doi.org/10.1051/limn/2009018

Burman, A. J., Hedger, R. D., Hellström, J. G. I., Andersson, A. G., & Sundt-Hansen, L. E. (2021). Modelling the downstream longitudinal effects of frequent hydropeaking on the spawning potential and stranding susceptibility of salmonids. *Science of The Total Environment*, *796*, 148999. https://doi.org/10.1016/J.SCITOTENV.2021.148999

Canadian Ministry of Justice. (1985). *Fisheries Act*. https://laws-lois.justice.gc.ca/eng/acts/f-14/

This article is protected by copyright. All rights reserved.

19360592, ja, Downloaded from https://onlinelibrary.wiley.com/doi/10.1002/eco.2530 by Institut National De La Recherche, Wiley Online Library on [16/02/2023]. See the Terms and Conditions (https://onlinelibrary.wiley.com/terms-and-conditions) on Wiley Online Library for rules of use; OA articles are governed by the applicable Creative Commons License

Casas-Mulet, R., Saltveit, S. J., & Alfredsen, K. T. (2016). Hydrological and thermal effects of hydropeaking on early life stages of salmonids: A modelling approach for implementing mitigation strategies. *Science of The Total Environment*, *573*, 1660–1672. https://doi.org/10.1016/J.SCITOTENV.2016.09.208

Chow, V. te. (1959). *Open Channel Hydraulics*. McGraw-Hill, New York. http://www.fsl.orst.edu/geowater/FX3/help/8_Hydraulic_Reference/Mannings_n_Tables.htm

Colomina, I., & Molina, P. (2014). Unmanned aerial systems for photogrammetry and remote sensing: A review. In *ISPRS Journal of Photogrammetry and Remote Sensing* (Vol. 92, pp. 79–97). Elsevier B.V. https://doi.org/10.1016/j.isprsjprs.2014.02.013

Enders, E. C., Watkinson, D. A., Ghamry, H., Mills, K. H., & Franzin, W. G. (2017). Fish age and size distributions and species composition in a large, hydropeaking Prairie River. *River Research and Applications*, *33*(8), 1246–1256. https://doi.org/10.1002/rra.3173

Environment Canada. (2013). *Measuring discharge with acoustic Doppler current profilers from a moving boat, version adapted for Water Survey of Canada*.

Environment Canada. (2015). *Real-Time Hydrometric Data Graph for SASKATCHEWAN RIVER BELOW TOBIN LAKE (05KD003) [SK] - Water Level and Flow - Environment Canada*. https://wateroffice.ec.gc.ca/report/real_time_e.html?stn=05KD003

ESA. (1973). *ESA - Endangered Species Act of 1973*. Department of the Interior, U.S. Fish and Wildlife Service. Washington, D.C. 20240. http://www.nmfs.noaa.gov/pr/pdfs/laws/esa.pdf

Federal Water Pollution Control Act. (2002). *Federal Water pollution Control Act*. United States Environmental Protection Agency. https://www.epa.gov/sites/production/files/2017-08/docu- ments/federal-water-pollution-control-act-508full.pdf.

FPA. (1920). *Federal Power Act - FPA*. U.S. Code, Federal Regulation and Development of Power. Chapter 12; Subchapter I, Regulation of the Development of Water Power and Re- Sources. https://www.fws.gov/laws/lawsdigest/FEDPOWR.HTML

Führer, S., Hayes, D. S., Hasler, T., Graf, D. R. M., Fauchery, E., Mameri, D., Schmutz, S., & Auer, S. (2022). Stranding of larval nase (Chondrostoma nasus L.) depending on bank slope, down-ramping rate and daytime. *Frontiers in Environmental Science*, *10*, 1275. https://doi.org/10.3389/FENVS.2022.966418/BIBTEX

Ghanem, A. H. M. (1995). *Two-dimensional finite element modeling of flow in aquatic habitats*. https://doi.org/10.7939/R3VH5CS4G

Glowa, S. E., Watkinson, D. A., Jardine, T. D., & Enders, E. C. (2022). Evaluating the risk of fish stranding due to hydropeaking in a large continental river. River Research and Applications, 1–16. https://doi.org/10.1002/rra.408316

Green, D. J., Duffy, M., Janz, D. M., McCullum, K., Carrière, G., & Jardine, T. D. (2016). Historical and Contemporary Patterns of Mercury in a Hydroelectric Reservoir and Downstream Fishery: Concentration Decline in Water and Fishes. *Archives of Environmental Contamination and Toxicology*, *71*(2), 157–170. https://doi.org/10.1007/s00244-016-0287-3

Green, D. J., Jardine, T. D., Weber, L. P., & Janz, D. M. (2020). Energy stores and mercury concentrations in a common minnow (spottail shiner, Notropis hudsonius) associated with a peaking hydroelectric dam. *River Research and Applications*, *36*(7), 1046–1055. https://doi.org/10.1002/rra.3625

Hauer, C., Unfer, G., Holzapfel, P., Haimann, M., & Habersack, H. (2014). Impact of channel bar form and grain size variability on estimated stranding risk of juvenile brown trout during hydropeaking. *Earth Surface Processes and Landforms*, *39*(12), 1622–1641. https://doi.org/10.1002/ESP.3552

This article is protected by copyright. All rights reserved.

19360592, ja, Downloaded from https://onlinelibrary.wiley.com/doi/10.1002/eco.2530 by Institut National De La Recherche, Wiley Online Library on [16/02/2023]. See the Terms and Conditions (https://onlinelibrary.wiley.com/terms-and-conditions) on Wiley Online Library for rules of use; OA articles are governed by the applicable Creative Commons License

Hayes, D. S., Moreira, M., Boavida, I., Haslauer, M., Unfer, G., Zeiringer, B., Greimel, F., Auer, S., Ferreira, T., & Schmutz, S. (2019). *Life Stage-Specific Hydropeaking Flow Rules*. https://doi.org/10.3390/su11061547

Hayes, D. S., Schülting, L., Carolli, M., Greimel, F., Batalla, R. J., & Casas-Mulet, R. (2022). Hydropeaking: Processes, Effects, and Mitigation. *Encyclopedia of Inland Waters*, 134–149. https://doi.org/10.1016/B978-0-12-819166-8.00171-7

Irvine, R. L., Oussoren, T., Baxter, J. S., & Schmidt, D. C. (2009). The effects of flow reduction rates on fish stranding in British Columbia, Canada. *River Research and Applications*, *25*(4), 405–415. https://doi.org/10.1002/RRA.1172

Javernick, L., Brasington, J., & Caruso, B. (2014). Modeling the topography of shallow braided rivers using Structure-from-Motion photogrammetry. *Geomorphology*, *213*, 166–182. https://doi.org/10.1016/j.geomorph.2014.01.006

Juárez, A., Adeva-Bustos, A., Alfredsen, K., & Dønnum, B. O. (2019). Performance of a two-dimensional hydraulic model for the evaluation of stranding areas and characterization of rapid fluctuations in hydropeaking rivers. *Water (Switzerland)*, *11*(2). https://doi.org/10.3390/w11020201

Korman, J., & Campana, S. E. (2009). Effects of Hydropeaking on Nearshore Habitat Use and Growth of Age-0 Rainbow Trout in a Large Regulated River. *Transactions of the American Fisheries Society*, *138*(1), 76–87. https://doi.org/10.1577/T08-026.1

Larrieu, K. G., & Pasternack, G. B. (2021). Automated analysis of lateral river connectivity and fish stranding risks. Part 2: Juvenile Chinook salmon stranding at a river rehabilitation site. *Ecohydrology*, *14*(6), e2303. https://doi.org/10.1002/ECO.2303

Larrieu, K. G., Pasternack, G. B., & Schwindt, S. (2021). Automated analysis of lateral river connectivity and fish stranding risks—Part 1: Review, theory and algorithm. *Ecohydrology*, *14*(2), e2268. https://doi.org/10.1002/ECO.2268

Leon, J. X., Roelfsema, C. M., Saunders, M. I., & Phinn, S. R. (2015). Measuring coral reef terrain roughness using "Structure-from-Motion" close-range photogrammetry. *Geomorphology*, *242*, 21–28. https://doi.org/10.1016/j.geomorph.2015.01.030

MacKinnon, B. D., Sagin, J., Baulch, H. M., Lindenschmidt, K. E., & Jardine, T. D. (2015). Influence of hydrological connectivity on winter limnology in floodplain lakes of the Saskatchewan River Delta, Saskatchewan. *Canadian Journal of Fisheries and Aquatic Sciences*, *73*(1), 140–152. https://doi.org/10.1139/cjfas-2015-0210

Mandlburger, G., Hauer, C., Wieser, M., & Pfeifer, N. (2015). Topo-Bathymetric LiDAR for Monitoring River Morphodynamics and Instream Habitats—A Case Study at the Pielach River. *Remote Sensing 2015, Vol. 7, Pages 6160-6195*, *7*(5), 6160–6195. https://doi.org/10.3390/RS70506160

Mihalicz, J. E., Jardine, T. D., Baulch, H. M., & Phillips, I. D. (2019). Seasonal effects of a hydropeaking dam on a downstream benthic macroinvertebrate community. *River Research and Applications*, *35*(6), 714–724. https://doi.org/10.1002/RRA.3434

Moore, K. M. S., & Gregory, S. v. (2011). Summer Habitat Utilization and Ecology of Cutthroat Trout Fry (Salmo clarki) in Cascade Mountain Streams. *Https://Doi.Org/10.1139/F88-224*, *45*(11), 1921–1930. https://doi.org/10.1139/F88-224

Moreira, M., Hayes, D. S., Boavida, I., Schletterer, M., Schmutz, S., & Pinheiro, A. (2019). Ecologically-based criteria for hydropeaking mitigation: A review. *Science of The Total Environment*, *657*, 1508–1522. https://doi.org/10.1016/J.SCITOTENV.2018.12.107

Moreira, M., Schletterer, M., Quaresma, A., Boavida, I., & Pinheiro, A. (2020a). New insights into hydropeaking mitigation assessment from a diversion hydropower plant: The GKI project (Tyrol, Austria). *Ecological Engineering*, *158*(April). https://doi.org/10.1016/j.ecoleng.2020.106035

This article is protected by copyright. All rights reserved.

19360592, ja, Downloaded from https://onlinelibrary.wiley.com/doi/10.1002/eco.2530 by Institut National De La Recherche, Wiley Online Library on [16/02/2023]. See the Terms and Conditions (https://onlinelibrary.wiley.com/terms-and-conditions) on Wiley Online Library for rules of use; OA articles are governed by the applicable Creative Commons License

Moreira, M., Schletterer, M., Quaresma, A., Boavida, I., & Pinheiro, A. (2020b). New insights into hydropeaking mitigation assessment from a diversion hydropower plant: The GKI project (Tyrol, Austria). *Ecological Engineering*, *158*. https://doi.org/10.1016/j.ecoleng.2020.106035

Nagrodski, A., Raby, G. D., Hasler, C. T., Taylor, M. K., & Cooke, S. J. (2012). Fish stranding in freshwater systems: Sources, consequences, and mitigation. *Journal of Environmental Management*, *103*, 133–141. https://doi.org/10.1016/J.JENVMAN.2012.03.007

Nelson, P. (2010). *Assessment of fish stranding effects at E. B. Campbell Hydroelectric Station.*

Nelson, P. A., Johnson, M. W., & Larter, J. L. (2009). *Assessment of Fish Stranding Effects at E.B. Campbell Hydroelectric Facility*.

Puffer, M., Berg, O. K., Einum, S., Saltveit, S. J., & Forseth, T. (2017). Energetic Consequences of Stranding of Juvenile Atlantic Salmon (Salmo salar L.). *Journal of Water Resource and Protection*, *09*(02), 163–182. https://doi.org/10.4236/jwarp.2017.92012

Sammons, S. M., & Bettoli, P. W. (2011). Population Dynamics of a Reservoir Sport Fish Community in Response to Hydrology. *North American Journal of Fisheries Managment*, *20*(3), 791–800.

Sauterleute, J. F., Hedger, R. D., Hauer, C., Pulg, U., Skoglund, H., Sundt-Hansen, L. E., Bakken, T. H., & Ugedal, O. (2016). Modelling the effects of stranding on the Atlantic salmon population in the Dale River, Norway. *Science of The Total Environment*, *573*, 574–584. https://doi.org/10.1016/J.SCITOTENV.2016.08.080

Smith, N. D., Morozova, G. S., Pérez-Arlucea, M., Gibling, M. R., Smith, N. D., Morozova, G. S., Pérez-Arlucea, M., & Gibling, M. R. (2016). Dam-induced and natural channel changes in the Saskatchewan River below the E.B. Campbell Dam, Canada. *Geomo*, *269*, 186–202. https://doi.org/10.1016/J.GEOMORPH.2016.06.041

Stewart, K., & Watkinson, D. A. (Douglas A.). (2004). *The freshwater fishes of Manitoba*. 278.

Teledyne RD Instruments. (2016). *WinRiver II – Software User's Guide, San Diego, CA, Teledyne RD Instruments, P/N 957–6231–00*.

Thi, L., Ha, T. H. U., Anh, T. T., & Bui, X. (2020). Experimental Investigation on the Performance of DJI Phantom 4 RTK in the PPK Mode for 3D Mapping Open-Pit Mines. *Journal of the Polish Mineral Engineering Society*, 65–74.

Tinkham, W. T., & Swayze, N. C. (2021). Influence of agisoft metashape parameters on uas structure from motion individual tree detection from canopy height models. *Forests*, *12*(2), 1–14. https://doi.org/10.3390/F12020250

Tuhtan, J. A., Noack, M., & Wieprecht, S. (2012). Estimating stranding risk due to hydropeaking for juvenile European grayling considering river morphology. *KSCE Journal of Civil Engineering*, *16*(2), 197–206. https://doi.org/10.1007/S12205-012-0002-5

Vaca-Jiménez, S., Gerbens-Leenes, P. W., & Nonhebel, S. (2020). The monthly dynamics of blue water footprints and electricity generation of four types of hydropower plants in Ecuador. *Science of The Total Environment*, *713*, 136579. https://doi.org/10.1016/J.SCITOTENV.2020.136579

Valentin, S., Lauters, F., Sabaton, C., Breil, P., & Souchon, Y. (1996). *Modelling temporal variations of physical habitat for brown trout (salmo trutta) in hydropeaking conditions*. *12*, 317–330. https://doi.org/10.1002/(SICI)1099-1646(199603)12:2/3

This article is protected by copyright. All rights reserved.

19360592, ja, Downloaded from https://onlinelibrary.wiley.com/doi/10.1002/eco.2530 by Institut National De La Recherche, Wiley Online Library on [16/02/2023]. See the Terms and Conditions (https://onlinelibrary.wiley.com/terms-and-conditions) on Wiley Online Library for rules of use; OA articles are governed by the applicable Creative Commons License

Vanzo, D., Tancon, M., Zolezzi, G., Alfredsen, K., & Siviglia, A. (2016). A modeling approach for the quantification of fish stranding risk: the case of lundesokna river (Norway). *Engineers Australia*, *11*, 326–333.

Watkinson, D. A., Ghamry, H. K., & Enders, E. C. (2020). *Canadian Science Advisory Secretariat (CSAS) Information to support the assessment of the Instream Flow Needs for Fish and Fish Habitat in the Saskatchewan River downstream of the E.B. Campbell Hydroelectric Station*. http://www.dfo-mpo.gc.ca/csas-sccs/

Wentworth, C. K. (1922). *A Scale of grade and class terms for clastic sediments*.

Young, P. S., Cech, J. J., & Thompson, L. C. (2011). Hydropower-related pulsed-flow impacts on stream fishes: A brief review, conceptual model, knowledge gaps, and research needs. *Reviews in Fish Biology and Fisheries*, *21*(4), 713–731. https://doi.org/10.1007/S11160-011-9211-0/TABLES/2

Zarfl, C., Lumsdon, A. E., Berlekamp, J., Tydecks, L., & Tockner, K. (2015). A global boom in hydropower dam construction. *Aquatic Sciences*, *77*(1), 161–170. https://doi.org/10.1007/S00027-014-0377-0

Accepted Article

This article is protected by copyright. All rights reserved.

19360592, ja, Downloaded from https://onlinelibrary.wiley.com/doi/10.1002/eco.2530 by Institut National De La Recherche, Wiley Online Library on [16/02/2023]. See the Terms and Conditions (https://onlinelibrary.wiley.com/terms-and-conditions) on Wiley Online Library for rules of use; OA articles are governed by the applicable Creative Commons License

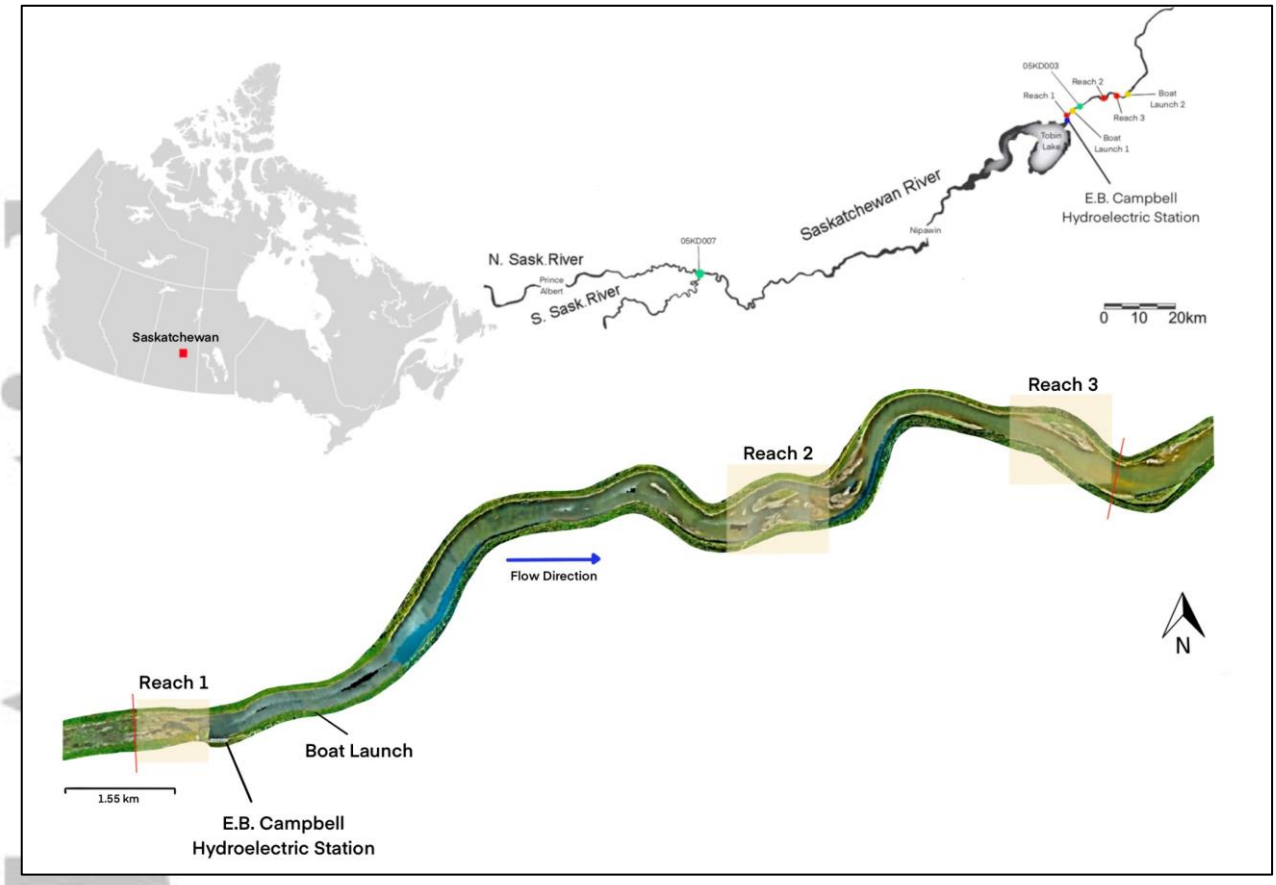

Figure 1 Map of study locations in the Saskatchewan River, Saskatchewan, Canada. E.B. Campbell Generating Station (N 53.411871 W 103.204802) located at beginning of ~16 km study reach. Reach 1 is in the spillway, the pre-existing river channel and is back watered daily by the hydropeaking regime, allowing for fish stranding to occur. Reach 2 ~9 km downstream the hydroelectric station. Reach 3 ~13 km downstream the hydroelectric station. Red lines characterize the upper and lower boundary of the 16 km study reach.

This article is protected by copyright. All rights reserved.

19360592, ja, Downloaded from https://onlinelibrary.wiley.com/doi/10.1002/eco.2530 by Institut National De La Recherche, Wiley Online Library on [16/02/2023]. See the Terms and Conditions (https://onlinelibrary.wiley.com/terms-and-conditions) on Wiley Online Library for rules of use; OA articles are governed by the applicable Creative Commons License

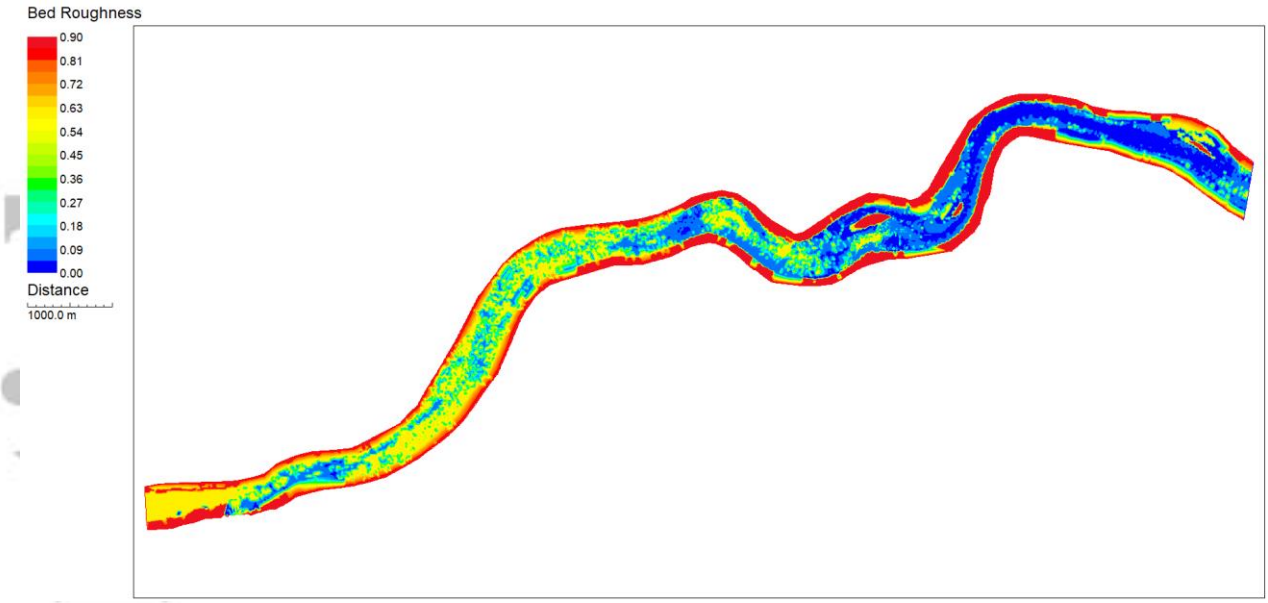

Figure 2 Roughness map of the ~16 km study reach downstream of the E.B. Campbell Hydroelectric Station, Saskatchewan River, Saskatchewan, Canada. Substrate roughness values: fine sand 0.0013 m, pebble 0.033 m, hard packed substrate 0.064 m, boulder 0.628 m, vegetation 0.628 m, and treed 0.9 m (Chow, 1959), reflected in the bed roughness legend.

Accepted Article

This article is protected by copyright. All rights reserved.

19360592, ja, Downloaded from https://onlinelibrary.wiley.com/doi/10.1002/eco.2530 by Institut National De La Recherche, Wiley Online Library on [16/02/2023]. See the Terms and Conditions (https://onlinelibrary.wiley.com/terms-and-conditions) on Wiley Online Library for rules of use; OA articles are governed by the applicable Creative Commons License

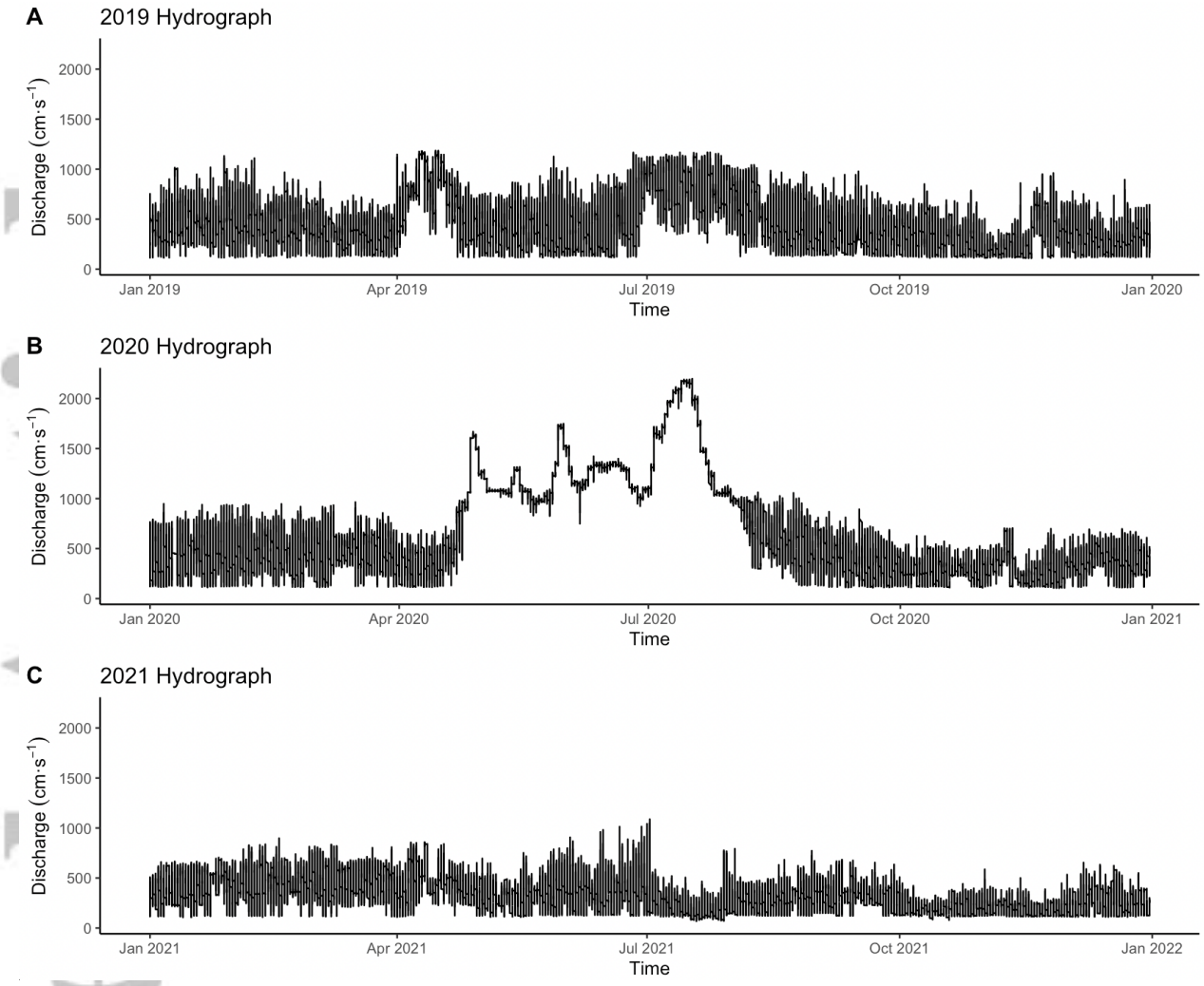

Figure 3 Hydrograph during three selected years at the E.B. Campbell Hydroelectric Station, measured at the Canada Water Survey gauge 05KD003. (A) Hydrography for 2019, representing an average flow year. (B) Hydrograph for 2020, representing a high flow year. (C) Hydrograph of 2021, representing a low flow year. Time series frequency is 5 min.

Accepted

This article is protected by copyright. All rights reserved.

19360592, ja, Downloaded from https://onlinelibrary.wiley.com/doi/10.1002/eco.2530 by Institut National De La Recherche, Wiley Online Library on [16/02/2023]. See the Terms and Conditions (https://onlinelibrary.wiley.com/terms-and-conditions) on Wiley Online Library for rules of use; OA articles are governed by the applicable Creative Commons License

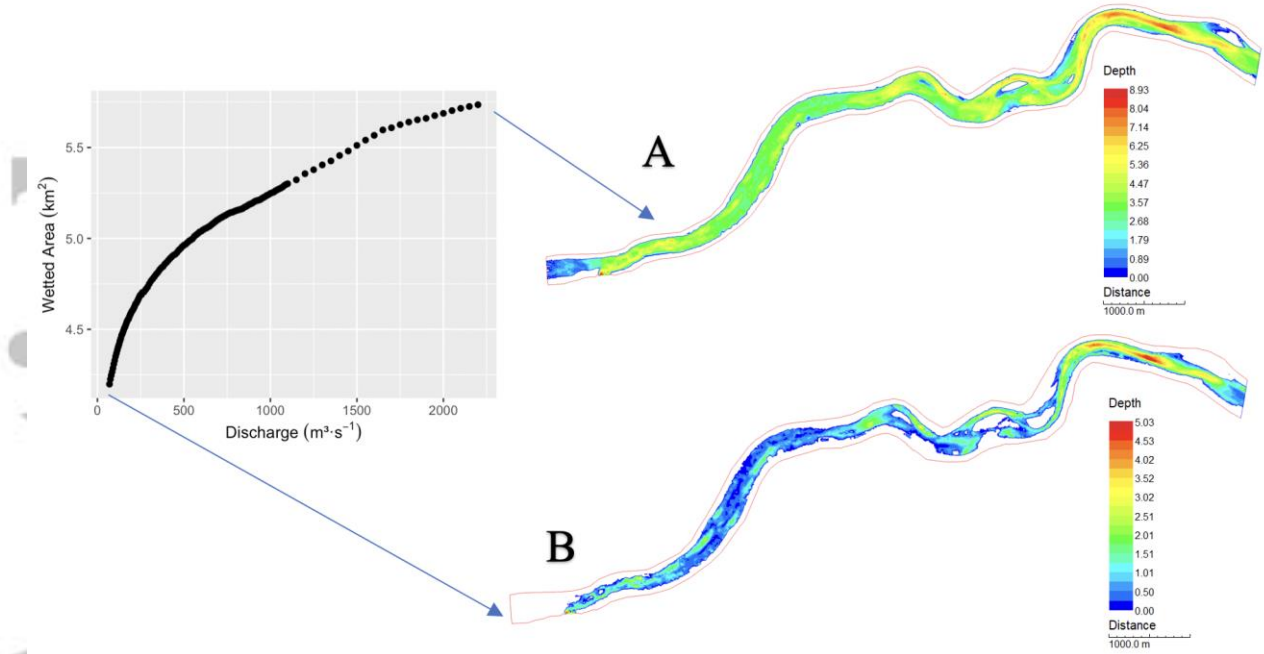

Figure 4 Modelled wetted area (km^2) downstream of the E.B. Campbell Hydroelectric Station, Saskatchewan River, Saskatchewan, Canada under two discharge scenarios: (A) wetted area of maximum modelled discharge of 2,200 $m^3 \cdot s^{-1}$, (B) wetted area of minimum modelled discharge of 70 $m^3 \cdot s^{-1}$. Wetted area maps were created in River2D characterizing the water's edge (dark blue outline), water depth (contoured colours), and model boundaries (red line) at low and high discharges of E. B. Campbell Hydroelectric Station.

Accepted

This article is protected by copyright. All rights reserved.

19360592, ja, Downloaded from https://onlinelibrary.wiley.com/doi/10.1002/eco.2530 by Institut National De La Recherche, Wiley Online Library on [16/02/2023]. See the Terms and Conditions (https://onlinelibrary.wiley.com/terms-and-conditions) on Wiley Online Library for rules of use; OA articles are governed by the applicable Creative Commons License

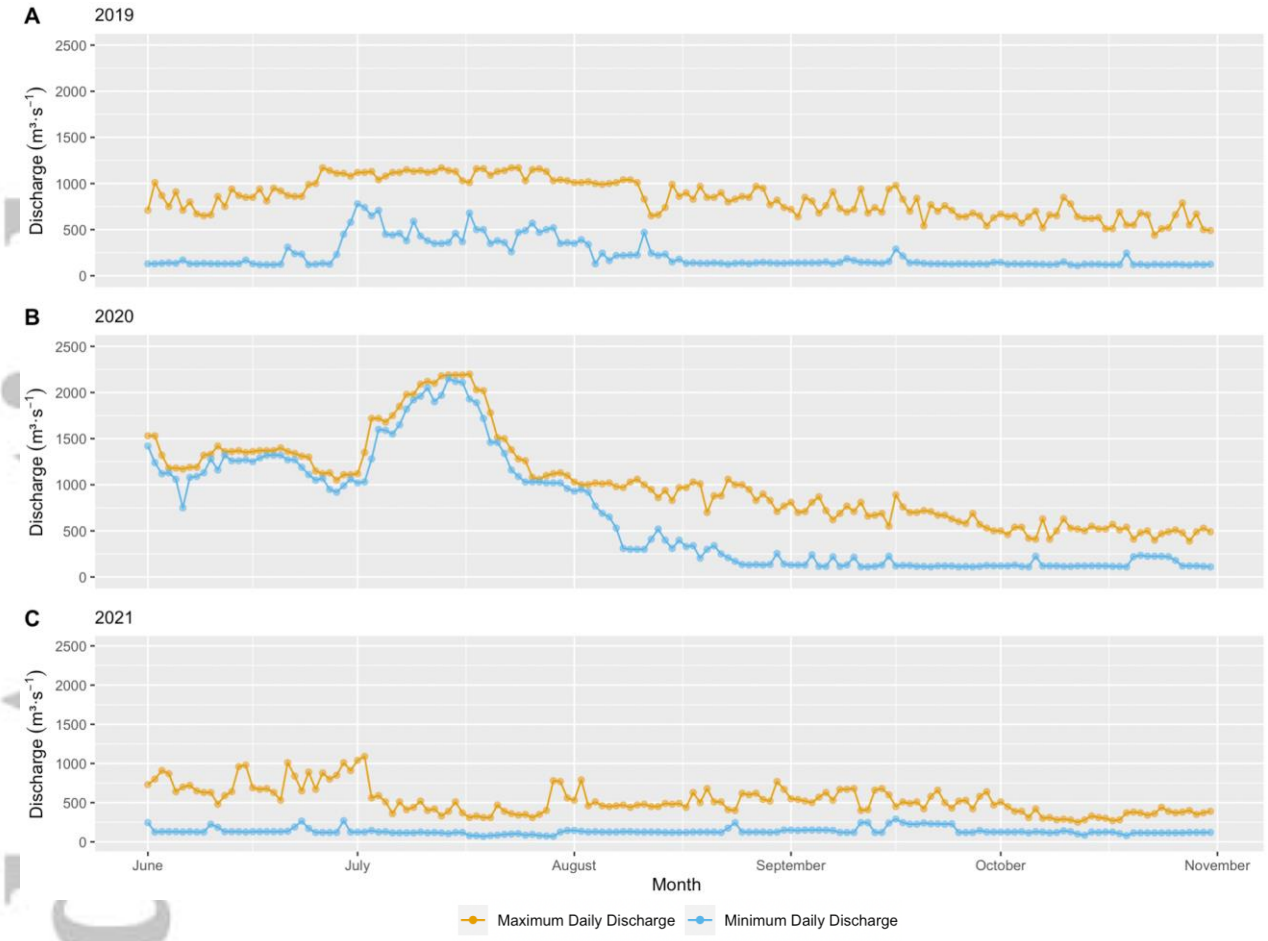

Figure 5 Recorded daily maximum and minimum discharges ($m^3 \cdot s^{-1}$) downstream of E.B. Campbell Hydroelectric station, Saskatchewan River, Saskatchewan, Canada witnessed in the study period, June – October for (A) 2019, (B) 2020, (C) 2021.

Accepted

This article is protected by copyright. All rights reserved.

19360592, ja, Downloaded from https://onlinelibrary.wiley.com/doi/10.1002/eco.2530 by Institut National De La Recherche, Wiley Online Library on [16/02/2023]. See the Terms and Conditions (https://onlinelibrary.wiley.com/terms-and-conditions) on Wiley Online Library for rules of use; OA articles are governed by the applicable Creative Commons License

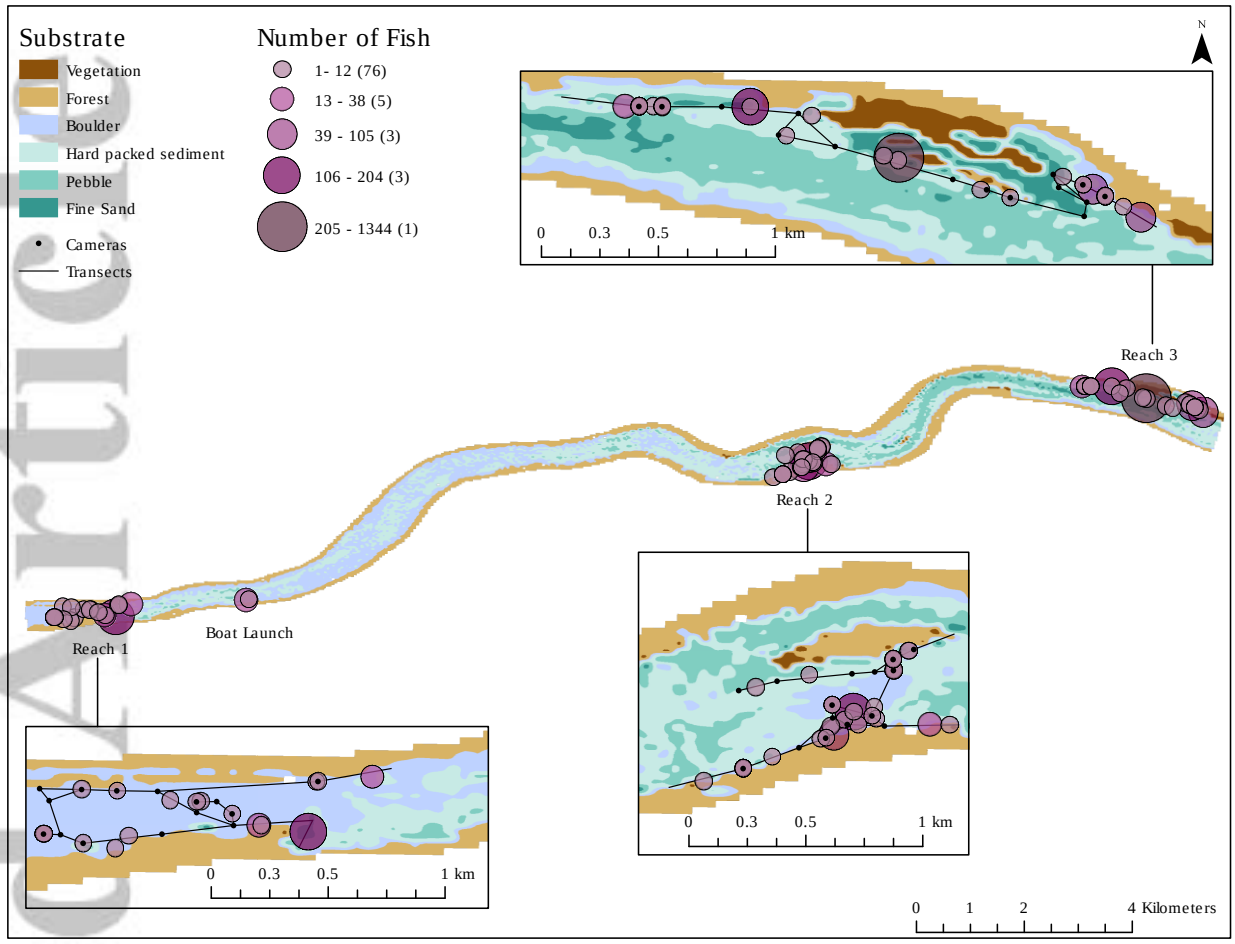

Figure 6 Overview of the substrate for the ~16 km study reach on the Saskatchewan River, Saskatchewan, Canada. Insets show closer visuals of each of the three reaches: Reach 1, Reach 2, and Reach 3. Map contours define the small substrate types of sand, pebble, hard pack substrate, and larger substrate (boulder) as well as forest and vegetation areas. Bubbles indicate the number of fish observed at each reach along transects during May to October 2021, each circle representing an observation of a stranded fish. A total of 2,493 stranded fish were recorded. Black dots symbolize the camera locations, black lines signify the transect monitoring locations.

This article is protected by copyright. All rights reserved.

19360592, ja, Downloaded from https://onlinelibrary.wiley.com/doi/10.1002/eco.2530 by Institut National De La Recherche, Wiley Online Library on [16/02/2023]. See the Terms and Conditions (https://onlinelibrary.wiley.com/terms-and-conditions) on Wiley Online Library for rules of use; OA articles are governed by the applicable Creative Commons License

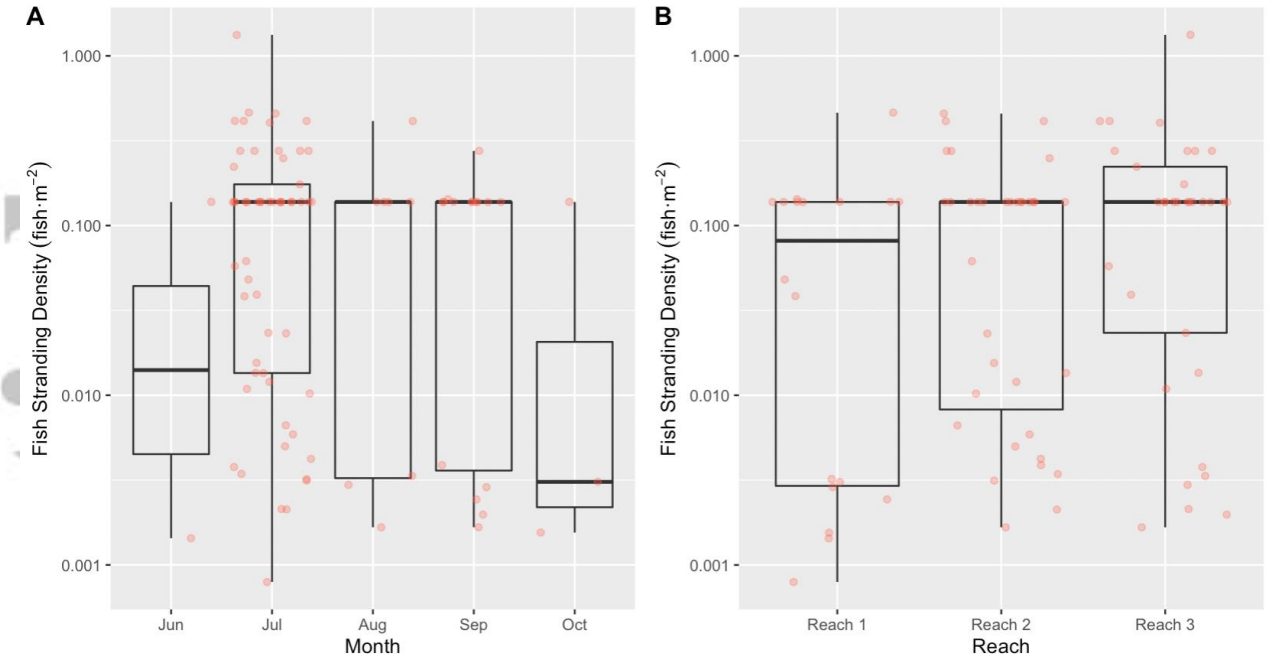

Figure 7 Fish stranding densities (fish·m^{-2}) observed using combined remote photography and transect monitoring with respect to predictor variables (A) observation month and (B) reach. **Note:** Y-axis is on a logarithmic scale.

Accepted Article

This article is protected by copyright. All rights reserved.

19360592, ja, Downloaded from https://onlinelibrary.wiley.com/doi/10.1002/eco.2530 by Institut National De La Recherche, Wiley Online Library on [16/02/2023]. See the Terms and Conditions (https://onlinelibrary.wiley.com/terms-and-conditions) on Wiley Online Library for rules of use; OA articles are governed by the applicable Creative Commons License

Table 1 Summary of the number of times discharges of E.B. Campbell Hydroelectric Station were below 100, 150, 200, and 250 $m^3 \cdot s^{-1}$ and discharges greater than 1,000 $m^3 \cdot s^{-1}$ during June to October in 2019, 2020, and 2021.

Year	<75 $m^3 \cdot s^{-1}$	<100 $m^3 \cdot s^{-1}$	< 150 $m^3 \cdot s^{-1}$	< 200 $m^3 \cdot s^{-1}$	< 250 $m^3 \cdot s^{-1}$	> 1,000 $m^3 \cdot s^{-1}$
2019 (avg. flow)	0	0	94	101	114	47
2020 (high flow)	0	0	56	58	72	75
2021 (low flow)	3	15	133	137	150	4

Accepted Article

This article is protected by copyright. All rights reserved.

19360592, ja, Downloaded from https://onlinelibrary.wiley.com/doi/10.1002/eco.2530 by Institut National De La Recherche, Wiley Online Library on [16/02/2023]. See the Terms and Conditions (https://onlinelibrary.wiley.com/terms-and-conditions) on Wiley Online Library for rules of use; OA articles are governed by the applicable Creative Commons License

Table 2 Summary of the stranded fish species during transect monitoring. Percentage of each species from the total number of stranded fish.

Scientific Name	Common Name	Number stranded	Percentage of stranded total (%)	Estimated number stranded in 2021
Notropis heterodon	Blacknose Shiner	2	0.09	1,300 ± 400
Lota lota	Burbot	2	0.09	1,300 ± 400
Coregonus artedi	Cisco	18	0.77	12,700 ± 3,600
Notropis atherinoides	Emerald Shiner	13	0.56	9,200 ± 2,600
Pimephales promelas	Fathead Minnow	9	0.39	6,300 ± 1,800
Etheostoma nigrum	Johnny Darter	3	0.13	2,100 ± 600
Percina caprodes	Logperch	11	0.47	7,700 ± 2,200
Esox lucius	Northern Pike	1	0.04	700 ± 200
Sander canadensis	Sauger	1	0.04	700 ± 200
Notropis hudsonius	Spottail Shiner	295	12.69	207,800 ± 59,400
Percopsis omiscomaycus	Troutperch	1	0.04	700 ± 200
	Unidentifiable	54	2.32	38,000 ± 10,900
Sander vitreus	Walleye	43	1.85	30,300 ± 8,700
Catostomus commersonii	White Sucker	1,627	69.98	1,146,200 ± 327,700
Perca flavescens	Yellow Perch	245	10.54	100,000 ± 49,300
Total:		**2,325**		**1,565,400 ± 21,700**

Accepted Article

This article is protected by copyright. All rights reserved.

19360592, ja, Downloaded from https://onlinelibrary.wiley.com/doi/10.1002/eco.2530 by Institut National De La Recherche, Wiley Online Library on [16/02/2023]. See the Terms and Conditions (https://onlinelibrary.wiley.com/terms-and-conditions) on Wiley Online Library for rules of use; OA articles are governed by the applicable Creative Commons License

Table 3 Summary of change in wetted history for the 16 km river reach downstream E.B. Campbell Hydroelectric Station during June to October in 2019, 2020, and 2021. Mean values presented with respective standard deviation.

Year	Mean Daily Change in Wetted Area (km^2)	Mean Daily Discharge ($m^3 \cdot s^{-1}$)		Daily Change in Discharge ($m^3 \cdot s^{-1}$)		
		Maximum	Minimum	Mean	Maximum	Minimum
2019 (avg. flow)	0.59 ± 0.16	854 ± 196	224 ± 154	626 ± 148	1,034	305
2020 (high flow)	0.35 ± 0.27	1,018 ± 469	660 ± 610	351 ± 227	868	38
2021 (low flow)	0.53 ± 0.15	530 ± 182	135 ± 41	394 ± 175	942	143

Accepted Article

This article is protected by copyright. All rights reserved.

19360592, ja, Downloaded from https://onlinelibrary.wiley.com/doi/10.1002/eco.2530 by Institut National De La Recherche, Wiley Online Library on [16/02/2023]. See the Terms and Conditions (https://onlinelibrary.wiley.com/terms-and-conditions) on Wiley Online Library for rules of use; OA articles are governed by the applicable Creative Commons License

Table 4 GLM results for combined remote photography and transect monitoring data with fish stranding density (fish·m^{-2}) as the response variable and the predictor variables month and reach. The fish stranding density was log transformed after a value of one was added to all data points. August and Reach 1 are taken as the default "reference" levels in the model.

Predictor Variables	Estimate	Standard Error	T-value	P value
Intercept	0.857	0.221	3.879	<0.001
June	-0.082	0.272	-0.300	0.764
July	1.581	0.241	6.566	<0.001
September	0.350	0.257	1.359	0.174
October	-0.147	0.353	-0.416	0.669
Reach 2	0.716	0.214	3.347	<0.001
Reach 3	0.527	0.209	2.528	0.011

Accepted Article

This article is protected by copyright. All rights reserved.

19360592, ja, Downloaded from https://onlinelibrary.wiley.com/doi/10.1002/eco.2530 by Institut National De La Recherche, Wiley Online Library on [16/02/2023]. See the Terms and Conditions (https://onlinelibrary.wiley.com/terms-and-conditions) on Wiley Online Library for rules of use; OA articles are governed by the applicable Creative Commons License

Table 5 Summary of the monthly fish stranding estimates, representing the area of stranding potential for each month for 2019, 2020, and 2021. Fish stranding densities used for calculating the monthly estimates of fish stranding and respective fish stranding estimate for remote photography and transect monitoring methodologies. Sum of stranded fish with respective standard deviation.

	Month	Cumulative Area of Stranding Potential (m^2)	Remote Photography		Transect Monitoring	
			Fish Stranding Density (fish/m^2)	Sum of Stranded Fish	Fish Stranding Density (fish/m^2)	Sum of Stranded Fish
2019	June	20,500	0.0002	5,000 ± 5,000	0.00004	900 ± 500
	July	11,540	0.0056	65,200 ± 13,900	0.0919	1,060,800 ± 302,600
	August	19,580	0.0014	27,400 ± 14,000	0.0004	7,200 ± 1,900
	September	19,200	0.0025	47,900 ± 14,700	0.0005	8,900 ± 2,900
	October	19,230	0.0007	12,700 ± 12,700	0.0002	4,800 ± 2,400
Total Stranded Fish				158,200 ± 60,200		1,082,500 ± 310,300
2020	June	1,810	0.0002	400 ± 400	0.00004	80 ± 50
	July	1,920	0.0056	10,900 ± 2,300	0.0919	176,800 ± 50,400
	August	13,470	0.0014	18,800 ± 9,600	0.0004	4,900 ± 1,300
	September	19,820	0.0025	49,400 ± 15,200	0.0005	9,200 ± 3,000
	October	15,500	0.0007	10,300 ± 10,200	0.0002	3,800 ± 2,00
Total Stranded Fish				89,800 ± 37,800		194,800 ± 56,800
2021	June	19,460	0.0002	4,800 ± 4,700	0.00004	800 ± 500
	July	17,640	0.0056	99,700 ± 21,300	0.0919	1,621,400 ± 462,400
	August	16,760	0.0014	234,300 ± 12,000	0.0004	6,100 ± 1,700
	September	13,770	0.0025	34,300 ± 10,500	0.0005	6,400 ± 2,100
	October	12,920	0.0007	8,600 ± 8,500	0.0002	3,200 ± 1,600
Total Stranded Fish				170,700 ± 57,000		1,638,000 ± 468,300

This article is protected by copyright. All rights reserved.

19360592, ja, Downloaded from https://onlinelibrary.wiley.com/doi/10.1002/eco.2530 by Institut National De La Recherche, Wiley Online Library on [16/02/2023]. See the Terms and Conditions (https://onlinelibrary.wiley.com/terms-and-conditions) on Wiley Online Library for rules of use; OA articles are governed by the applicable Creative Commons License